AIAA Guidance, Navigation, and Control Conference
2 - 5 August 2010, Toronto, Ontario Canada

AIAA 2010-8195

Development and Testing of a GNC-FDI Filter for a Reusable Launch Vehicle during Ascent

Murray L. Kerr[1], Andrés Marcos[2] and Luis F. Peñín[3]
Deimos Space S.L., Madrid, 28760, Spain

This paper presents the design process and evaluation of a GNC fault detection and isolation (GNC-FDI) filter for the provision of health monitoring capabilities on a reusable launch vehicle (RLV) during ascent. A high fidelity nonlinear model of the Hopper RLV forms the basis of the vehicle benchmark, with NDI control providing a robust vehicle response during unfaulted vehicle operation. Two faults and a variety of fault dynamics are considered; faults in the central engine gimbal actuator and the yaw rate sensor. A robust FDI filter design procedure is developed based on H-infinity FDI theory. Scheduling of designed LTI filters is employed to overcome the variation inherent in the vehicle's dynamical characteristics during ascent. A key feature of the developed design process is that FDI filters are designed in open-loop, despite the vehicle dynamics varying between stable and unstable during the ascent. Monte-Carlo analysis performed using nonlinear simulations demonstrates the robustness and effectiveness of the proposed FDI approach.

Nomenclature

d	= Disturbance
f	= Generic fault
f_s	= Sensor fault
f_a	= Actuator fault
$\hat{f}$, res	= Fault estimate
F	= FDI filter
F_Y,F_U	= FDI filter subelements
G	= Generic vehicle model
G_u	= Vehicle model element accepting plant input
G_d	= Vehicle model element accepting disturbance input
G_f	= Vehicle model element accepting fault input
K_a , K_s	= Fault location selectors
n	= Noise
u	= Plant input
y	= Plant output

I. Introduction

THIS paper presents the design process and evaluation of a GNC fault detection and isolation (GNC-FDI) filter for the provision of health monitoring capabilities on a reusable launch vehicle (RLV) during ascent. The work was performed within the European Space Agency (ESA) funded study entitled Health Management for Reusable-space Transportation (HMS). In the study, a high fidelity nonlinear model of the EADS Astrium Hopper RLV was employed as the vehicle benchmark, with nonlinear dynamic inversion (NDI) control providing a robust vehicle response during unfaulted vehicle operation.[1]

[1] Senior Control Engineer, Deimos Space. murray.kerr@deimos-space.com.
[2] Senior Control Engineer, Deimos Space.
[3] Project Manager and Head of GNC/AOCS Division, Deimos Space. Senior AIAA member.

In the HMS study faults were considered at several levels within the Hopper RLV and GNC system. This work considers faults acting at the GNC level, with faults active on both the sensors and actuators of the vehicle. The principal design problem is therefore to *detect* faulty behaviour of an actuator or sensor and *isolate* the fault to either the sensor or actuator. *Estimation* of the fault effects, to a level of accuracy suitable for the compensation of the fault effects (e.g. fault tolerant control) was also considered, but as a secondary objective.

For the HMS study, previous GNC-FDI filter design and assessment activities were reported in Ref.2 and Ref.3. These considered the problem of FDI during the re-entry period of the Hopper RLV trajectory, with the capability to perform actuator and sensor FDI demonstrated in simulation campaigns on the vehicle benchmark. The FDI problem considered in this paper is that of the ascent flight of the Hopper RLV, with the aim being to demonstrate similar FDI capabilities in this distinct phase of the flight. The fault scenario considered covers the period of the ascent flight corresponding to the first 130 seconds, which includes the key peak dynamic pressure phase of the flight. Two faults and a variety of fault dynamics were considered during this ascent period; abrupt and incipient faults in the central engine gimbal actuator and the yaw rate sensor.

This paper details the robust FDI filter design procedure that was developed for this fault scenario based on H-infinity FDI theory and its testing using the Hopper RLV simulator. In the design procedure LTI FDI filters were designed at trim points covering the ascent period and scheduling of these LTI FDI filters was employed to overcome the variation inherent in the vehicle's dynamical characteristics during ascent, with strong variation seen in the environmental parameters (Qdyn, Mach), vehicle attitude (flight path angle and angle-of-attack) and the vehicle MCI properties, due to the variation of inertia and CoG with consumed fuel mass.

Apart from the HMS project work reported in Ref.2 and Ref.3, previous work on the application of H-infinity FDI techniques to ascent and re-entry vehicles include Ref.4, where reaction control system failures were considered during the early re-entry phase of the Shuttle vehicle, Ref.5, which considered the Mathworks Shuttle vehicle model, operating in the transonic region of the re-entry trajectory, with actuator failures considered, and Ref.6 which considered faults acting on the Mathworks HL-20 vehicle benchmark during the final phase of re-entry flight (TAEM).

The paper is structured as follows. Section II presents the Hopper RLV, the fault scenarios and resulting FDI problem. Section III presents an overview of the filter design process, including a discussion of the design challenges. Section IV presents the evaluation of the designed filters for FDI on the Hopper using a high fidelity simulation environment and the statistical analysis of the results. Conclusions are detailed in Section V.

II. Problem Statement

A. NDI Controlled Hopper RLV Ascent

The Hopper RLV was designed by Astirum ST to perform sub-orbital point-to-point flights. In the present work, a focused time period within the ascent phase for the Hopper RLV flight is considered, with the vehicle controlled by an NDI controller[1] designed within the HMS study that ensures the vehicle robustly tracks a predefined ascent trajectory profile in heading and flight path angle. The time period considered is from 0 to 130 seconds, which corresponds to the period at the start of the ascent flight. The characteristics of the NDI controlled vehicle over this period of the ascent flight are shown in Figure 1 to Figure 6, which show an exemplary 50 random simulation runs for the ascent.

The rationale supporting the selection of this 130 second fault period can be summarised as follows:

- Over this period of the ascent flight the largest variation of the vehicle states occurs, with the majority of the variation in the flight path angle, angle-of-attack, Mach number and dynamic pressure occurring over this time period. Additionally, the dynamic pressure peaks during this ascent period.
- The effects of the mass variation over this period of flight are pronounced and account for over 50% of the x-axis CoG variation over the ascent, and large inertia changes (see Figure 5 and Figure 6).
- Over this flight period the aero surfaces, RCS and engine gimbal pitch and yaw actuators are all employed to actuate the vehicle, giving rise to a highly redundant actuation scheme (see e.g. Figure 4).
- The fact that the considered ascent period covers the initial ascent flight means that the final orbital injection is highly sensitive to failures during this time period, making the GNC-FDI problem particularly relevant.

- This focused time period corresponds to the period where the variation in the vehicle states and environmental conditions at a given time are large. As seen in Figure 1 to Figure 3, the angle-of-attack, velocity, altitude and dynamic pressure vary between plant cases.

These features of the chosen ascent flight period give rise to a challenging FDI problem and one that highlights some of the main challenges associated with designing FDI filters for this type of vehicle during the ascent phase. Section III.E highlights further these challenges considering the properties of the LTI models for the vehicle that are used for GNS-FDI filter design.

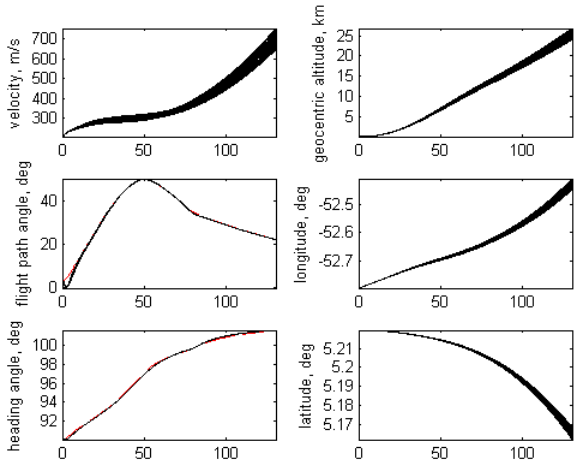

Figure 1. Ascent period (0-130 sec) translational response for 50 random ascent simulations.

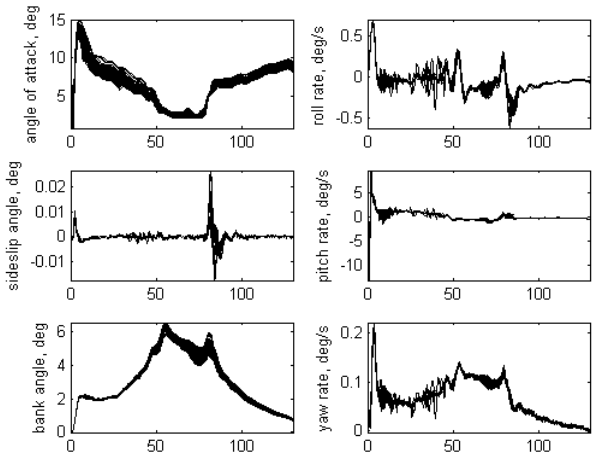

Figure 2. Ascent period (0-130 sec) rotational response for 50 random ascent simulations.

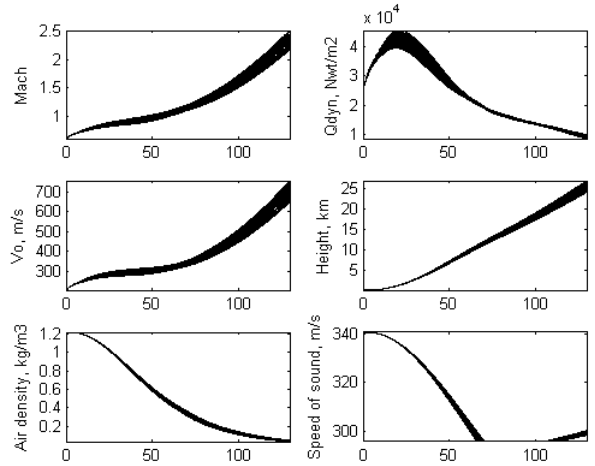

Figure 3. Ascent period (0-130 sec) environmental parameters for 50 random ascent simulations.

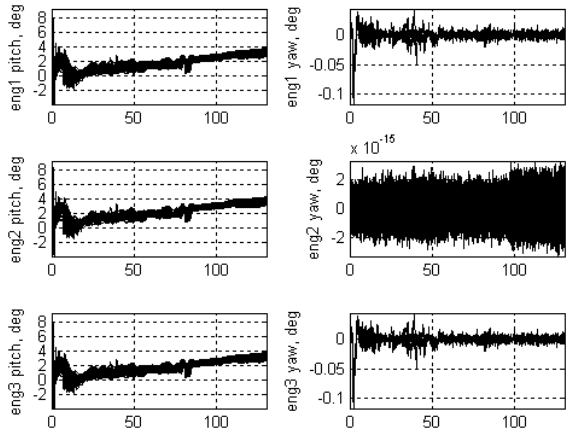

Figure 4. Ascent period (0-130 sec) engine gimbal deflections for 50 random ascent simulations.

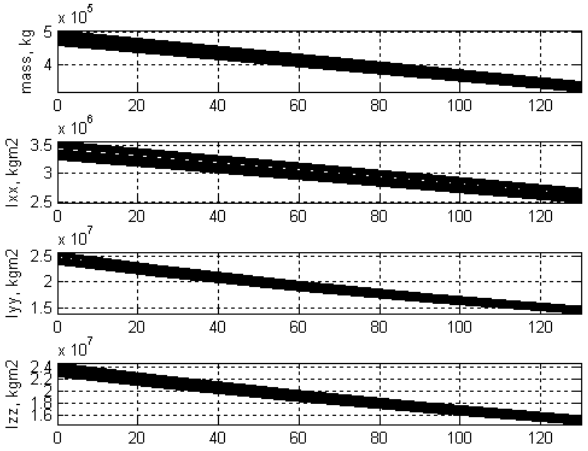

Figure 5. Ascent period (0-130 sec) mass and inertia for 50 random ascent simulations.

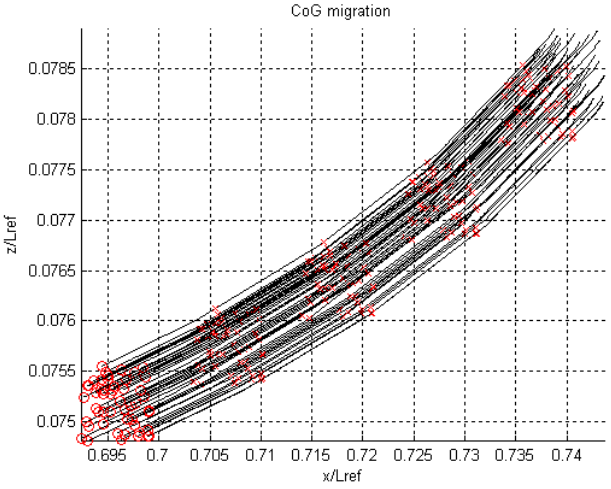

Figure 6. Ascent period (0-130 sec) CoG migration (o – initial; x at 30 second steps) for 50 random ascent simulations.

B. Selected Fault Scenarios

The following selection of faults for the ascent FDI problem was considered:

- Actuator: engine 2 (central) gimbal pitch actuator
- Sensor: yaw rate (r) sensor

These faults were chosen based on fault analysis performed,[7] their relevance to the ascent flight, and the requirement imposed in the HMS project that the GNC-FDI filter demonstrate detection of faults in one sensor and one actuator of the vehicle and that an IMU type fault be included in the fault set. Note that only independent fault cases are considered, in that only a single fault in either the sensor or actuator is considered. Furthermore, with both engine 2 gimbal pitch and yaw rate sensor faults considered, the faults effects on the vehicle response will be seen in both the longitudinal and lateral axes, with the engine 2 gimbal pitch expected to have a dominant effect on the longitudinal response and the yaw rate sensor on the lateral response of the vehicle.

The effects of faults in this actuator and sensor were analysed.[7] It was shown that the yaw rate sensor fault was a highly critical fault, with the controlled vehicle response highly sensitive to this fault. Conversely, due to the redundancy in the actuation scheme on the Hopper during ascent, the engine 2 gimbal pitch actuator fault was shown to be naturally accommodated in the controlled system and is only critical for large fault strengths.

While any type of fault could occur in the chosen actuator and sensor, to assess the effect of faults, it was necessary to limit the evaluation to a subset of the possible fault types. The following choice of fault type was made:

Engine 2 gimbal pitch:

- bias faults
- lock-in-place (LIP) faults

Yaw rate (r) sensor:

- bias faults
- drift faults

This choice includes faults that are abrupt, incipient and dynamic. In particular, the bias faults have a strong abrupt effect on the closed-loop vehicle response. Conversely, the drift fault is incipient and therefore easily accommodated when of a low strength, making fault detection difficult. The effect of the LIP fault depends on the commands in the gimbal actuator over the period of time the fault is active. For the Hopper ascent flight is was found that, due to the redundancy in the actuation scheme, engine 2 (central) gimbal actuator LIP fault effects are only very small, non-critical and too small to be detectable. Therefore, for the *remainder of the paper only bias faults will be considered in the gimbal.*

The following bias faults were proposed for testing, with the magnitude of the fault chosen such that the closed-loop system remains stable (as no reconfiguration capabilities are present in the system):

Bias fault in engine 2 gimbal pitch:

- 5 degrees, 50 seconds active.

Bias fault in yaw rate (r) sensor:

- 5 degrees/sec, 50 seconds active.

For the drift fault, the following was chosen:

Drift fault in yaw rate (r) sensor:

- drift, 0.01 degrees/s^2, active for the full 130s flight period.

The chosen fault types, strengths and activation periods will be used in the latter testing.

C. FDI Design Problem and Objectives

With the fault scenarios defined, the design problem is to design a filter capable of FDI of the gimbal actuator and raw rate sensor. Importantly, this should be done robustly, both to uncertainty effects and parameter variation effects. Full details of the uncertainty sources considered are provided in Ref.1. They can be summarized as:

- aerodynamic coefficient uncertainties as a function of Mach
- mass 5%
- inertia 5%
- x-,z-MRP 0.5%
- y-MRP 0.1%

The satisfaction robustly of these objectives will be assessed by Monte-Carlo analysis using nonlinear simulations of the high fidelity Hopper model and active GNC system. The current problem solution is restricted to the employment of an open-loop FDI architecture. This ensures the design process is independent of the controller, which is this instance appears necessary given the nonlinear (NDI) controller, and typically provides for reduced sensitivity to uncertainty. Here H-infinity FDI theory was chosen to design the filters, due to the importance of robustness and the ability to provide this systematically using H-infinity (LFT) theory.[8]

III. FDI filter design and scheduling

D. Open-loop Hopper RLV model

The full 6DOF nonlinear model reported in Ref.1 forms the basis for the model development. For the fault scenarios considered, representative models of the vehicle were developed to a level of fidelity suitable for FDI filter design. Due to the selection of faults affecting dominantly either the longitudinal or lateral vehicle response, LTI models were developed for the lateral and for longitudinal vehicle response based on the observed approximate decoupling of the lateral and longitudinal vehicle response modes. For both the lateral and longitudinal model development, the approach was to trim and linearise the plant at a number of trajectory points within the ascent flight period considered (0 to 130 seconds). These points were chosen during the filter design process, based on observations made when performing the scheduling of the filters.

The resulting linearised models for the Hopper vary between the longitudinal and lateral cases. The use of a decoupled model gives rise to a different number of states in the longitudinal and lateral models. Furthermore, it was observed that during the ascent flight, some actuators only had an effect on either that lateral or longitudinal response. Therefore, the models differ in both their states, and subsequent outputs, and their inputs. They can be summarized as follows.

The longitudinal LTI plant models consist of five states (pitch rate q, angle of attack α, velocity Vt, flight path angle γ, and geometric altitude R), five outputs (the states) and five inputs (effective outboard elevator, effective inboard elevator, engine 1 pitch gimbal, engine 2 pitch gimbal, engine 3 pitch gimbal).

The lateral LTI plant models consist of seven states (roll rate p, yaw rate r, sideslip angle β, bank angle σ, velocity Vt, heading angle and geometric altitude R), seven outputs (the states) and seven inputs (effective outboard aileron, effective inboard aileron, rudder, RCS-x, engine 1 yaw gimbal, engine 2 yaw gimbal, engine 3 yaw gimbal).

The LTI models provided by the trim and linearisation processes have some important characteristics, such as the variation of the plant dynamics with parametric uncertainty and over the flight period (parameter variation). These features are highlighted in the following figures. In addition to these quantitative changes, it is evident that the parameter variation and uncertainty is sufficient to also change the gross qualitative features of the vehicle behavior, with the stability of the vehicle seen to vary. Note that in the figures to follow, points in the ascent flight period are chosen with respect to the level of consumed fuel mass, as this is the variable used for scheduling of the FDI filters, as described in Section III.G.

Figure 7 shows the longitudinal vehicle model stability changes both over different periods of the ascent flight period and at each flight point, with some cases unstable and others stable. Changes in the natural frequency and damping of the vehicle modes are also evident.

Figure 9 and 10 show that, except for a few cases for the trim point with consumed mass of 2e4 kg, the lateral model is seen to be unstable over the full flight period. Changes in the natural frequency and damping of the vehicle modes are also evident.

Figure 8 provides a more detailed examination of the effect of parameter variation only on the *nominal* vehicle longitudinal response over the ascent flight period. It is seen that the vehicle's short period mode over the first 25 seconds of the flight varies between stable and unstable, then is stable over the next 80 seconds of flight, after which it becomes again unstable. The large change in the natural frequency and damping of this mode is also evident. For the lateral response (not shown), similar changes in natural frequency and damping are also evident, but no change in stability is seen, with the approximate lateral Dutch roll mode always unstable.

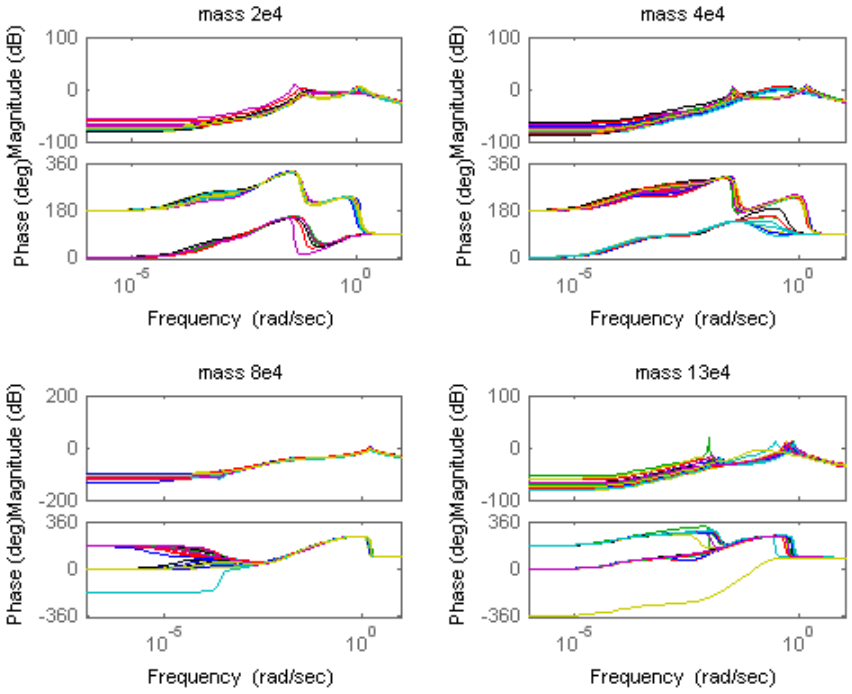

Figure 7. Effect of parameter uncertainty on the effective outer elevator to pitch rate (q) frequency response at four trim points in ascent flight at four flight conditions: 25 random plant cases.

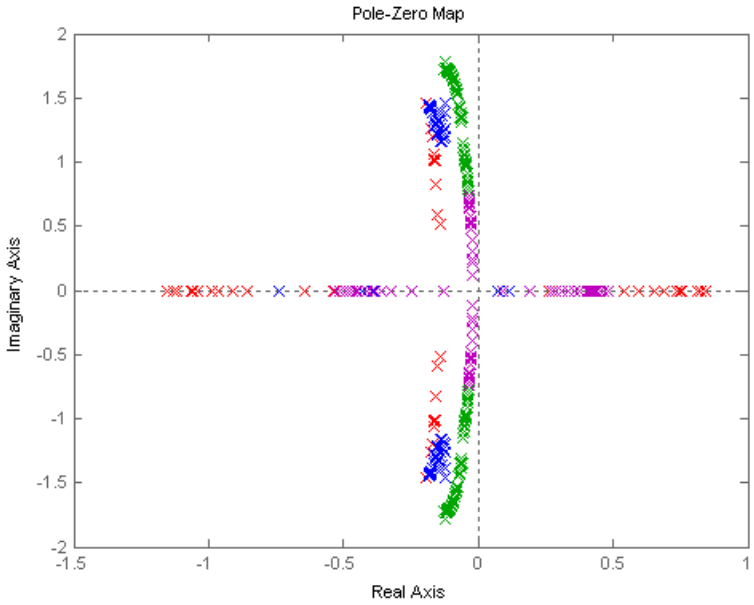

Figure 8. Migration of the longitudinal short period mode poles for the nominal trimmed vehicle (red – [0,20]s; blue – [20,50]s; green – [50,100]s; magenta – [100,130]s)

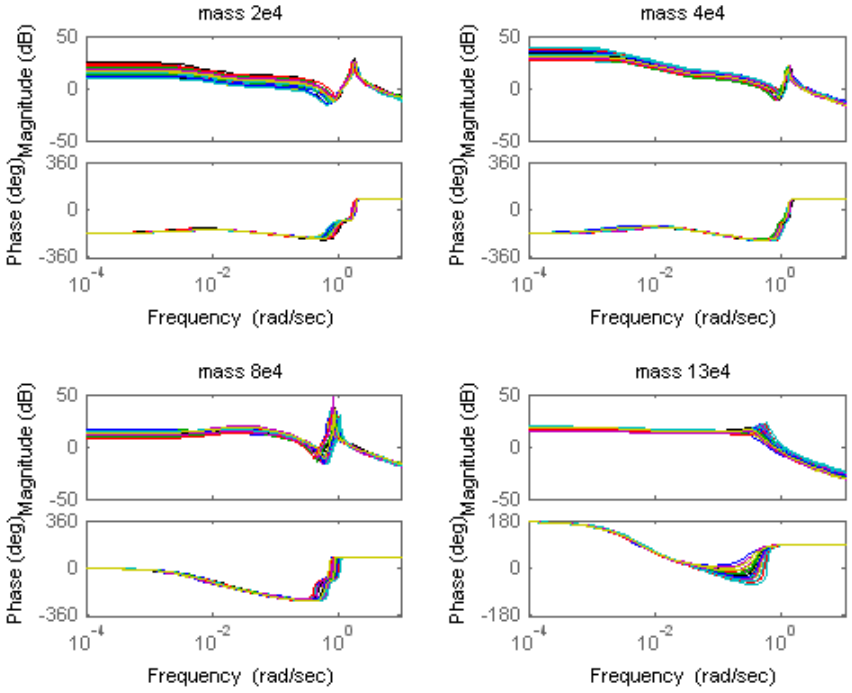

Figure 9. Effect of parameter uncertainty on the effective outer aileron to roll rate (p) frequency response at four trim points in ascent flight at four flight conditions: 25 random plant cases.

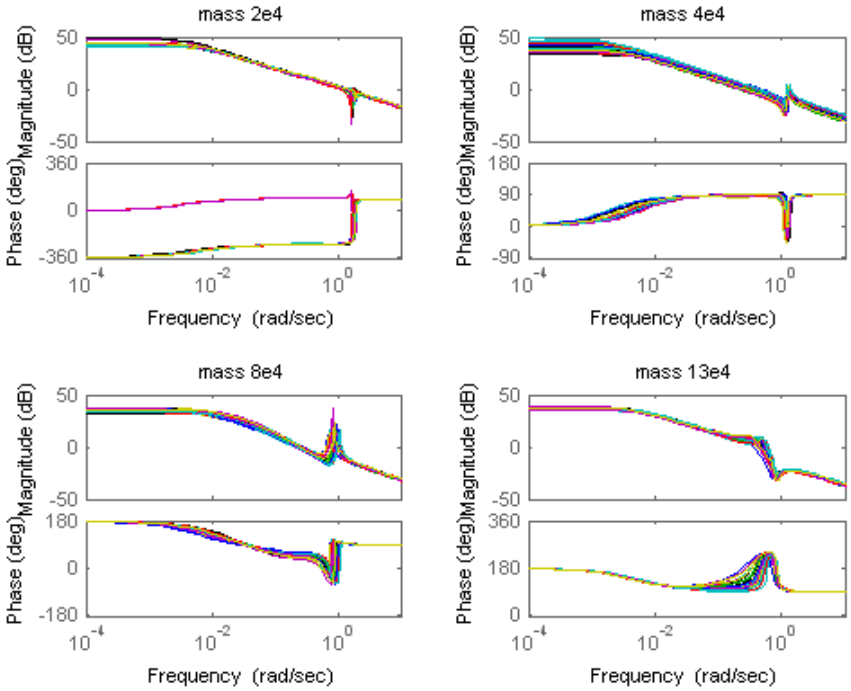

Figure 10. Effect of parameter uncertainty on the rudder to yaw rate (r) frequency response at four trim points in ascent flight at four flight conditions: 25 random plant cases.

E. GNC FDI Design Challenges

This subsection serves to summarise some of the challenges involved in designing a GNC-FDI filter for fault detection and isolation on the Hopper RLV during the considered ascent period. The challenges can be seen in the previous subsections and can be summarised as follows:

- Large plant dynamics variation during the ascent period due to parameter variation.
- Significant plant dynamics variation at points in the chosen ascent flight period due to uncertainty in the vehicle parameters.
- Varying stability of the plant dynamics over the flight period and with parameter uncertainty.

These challenges stem from the characteristics of the Hopper when tracking the present ascent trajectory,[1] and hence are inherent to the present GNC-FDI problem. The effect of these design challenges is different in the lateral and longitudinal design problems due to the varied effects of the parameter variations.

For the lateral design problem, the variation in the vehicle response characteristics is large but is mainly only quantitative, being changes in the damping and frequency of the vehicle modes. The qualitative vehicle characteristics do not change significantly, in that the unstable modes remain unstable throughout the flight period and similarly for the stable modes. Hence, while instability of the modes presents a fundamental limitation on the achievable performance of the filters[9] (particularly on the decoupling of exogenous inputs from the fault estimates), it does not preclude a successful design.

For the longitudinal design problem, the variation in the vehicle response characteristics are large and additionally, these changes are both quantitative and qualitative, being changes in the damping and frequency of the vehicle modes, and the stability of the modes and the number of real and complex modes. The latter principally occurs in the longitudinal response over the early flight period. These features combined lead to a very difficult design problem, which in some periods of the ascent flight may preclude a completely successful design.

Based on this discussion, it is reasonable to anticipate the longitudinal FDI design problem will be more difficult than the lateral problem. This is supported by the results in Section IV.

Remark: The FDI design problem for the re-entry phase of the Hopper RLV[2,3] is similar to the lateral FDI problem that is faced here, except that the parameter variation in the present problem is somewhat greater and the subsequent scheduling problem is more difficult. The longitudinal FDI problem faced here is significantly more difficult than that for the re-entry phase, for the reasons described above.

Remark: The above discussion of the design challenges was based on the independent consideration of the challenges that arise from parameter uncertainty and parameter variation. It was argued that it is the qualitative (gross) changes in the plant dynamics that are most problematic for the design of FDI filters at a given point and the scheduling of these filters. When the combined effect of the gross changes due to both the parameter variation and parametric uncertainty is considered, it is clear that the design problem will be very challenging, and the scheduling problem highly non-trivial and potentially very difficult over some periods of the flight.

F. Closed-loop and FDI architecture

The system under consideration can be represented as in Fig. 11. It consists of the Hopper vehicle, in closed-loop with the NDI controller, which is ensuring the vehicle tracks the reference trajectory. The Hopper vehicle response is subject to faults, and based on the commanded inputs to the vehicle (u) and sensed outputs (y), the GNC-FDI filter should detect and isolate the faults via the provided fault estimate signal $\hat{f}$.

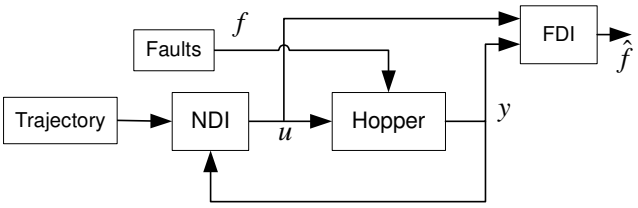

Figure 11. Closed-loop Hopper & FDI interconnection.

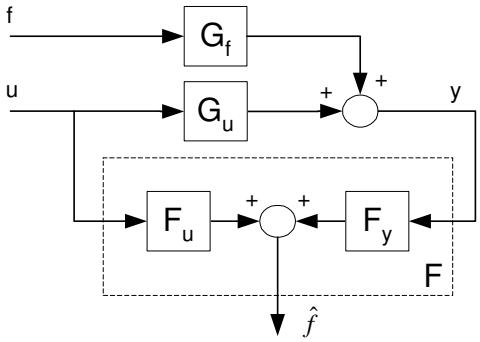

Figure 12. Basic FDI design architecture

With the GNC-FDI filter using the inputs and outputs of the vehicle only, this is an open-loop FDI architecture. Hence the GNC-FDI filter is to be designed based on only the LTI vehicle models, which are those obtained from the trim and linearisation process. Figure 12 shows this open-loop FDI problem more generically, with the fault estimate signal based on filters acting on both the sensed outputs and commanded inputs.

G. Design of LTI Filters and Scheduling

The FDI filters employed for fault detection and isolation are designed using the same design process as that detailed in Ref.2 and Ref.3. This design process solves a model-based open-loop FDI problem, as is depicted in Figure 12. The present solution to the model-based open-loop FDI problem is provided by H-infinity synthesis theory. This provides FDI filters that can solve the model-based open-loop FDI problem while providing some insensitivity of the fault estimate to uncertainty, disturbance and noise effects.

The FDI design problem can in the most part be posed as a standard H-infinity control problem in linear fraction transformation (LFT) form, with the system interconnection depicted in Figure 13 and Figure 14 for the longitudinal (actuator fault) and lateral (sensor fault) cases, respectively. The main modification to the standard H-infinity design approach is a change in the posing of the FDI problem to overcome the difficulties associated with designing on an unstable plant; namely those associated with designing, using H-infinity theory, an FDI filter that cannot stabilise the unstable plant.

In the design problem, once the interconnection is chosen in a manner suitable for H-infinity design, the key design choices are the weighting matrices denoted by W_*, which correspond to those standard in H-infinity FDI design and are employed to shape the FDI problem (see, e.g. Ref.8 and Ref.5). The gain matrices K_a and K_s correspond to selector matrices, which determine which input and output channels are affected by the actuator and sensor faults, respectively, here being the fourth longitudinal actuator (engine 2 pitch gimbal) and the second lateral sensor (yaw rate).

1. Engine 2 Pitch Gimbal Fault

The longitudinal FDI design problem is depicted in Figure 13. Here the plant model in LFT form is that for the longitudinal plant response at the chosen design point (trim point). Consistent with the longitudinal model of the vehicle, here the FDI filter takes as input the longitudinal actuator commands (effective outboard elevator, effective inboard elevator, engine 1 pitch gimbal, engine 2 pitch gimbal, engine 3 pitch gimbal) and a subset of the

longitudinal model outputs, being the sensed pitch rate q and angle of attack α. Note that the LFT plant model includes all five longitudinal states.

A solution to the FDI problem depicted in Figure 13 can be found using H-infinity design theory. The designed FDI filter F_a then takes 7 inputs (5 control inputs and 2 plant outputs) and outputs the scalar estimate of the fault acting on the engine 2 pitch gimbal.

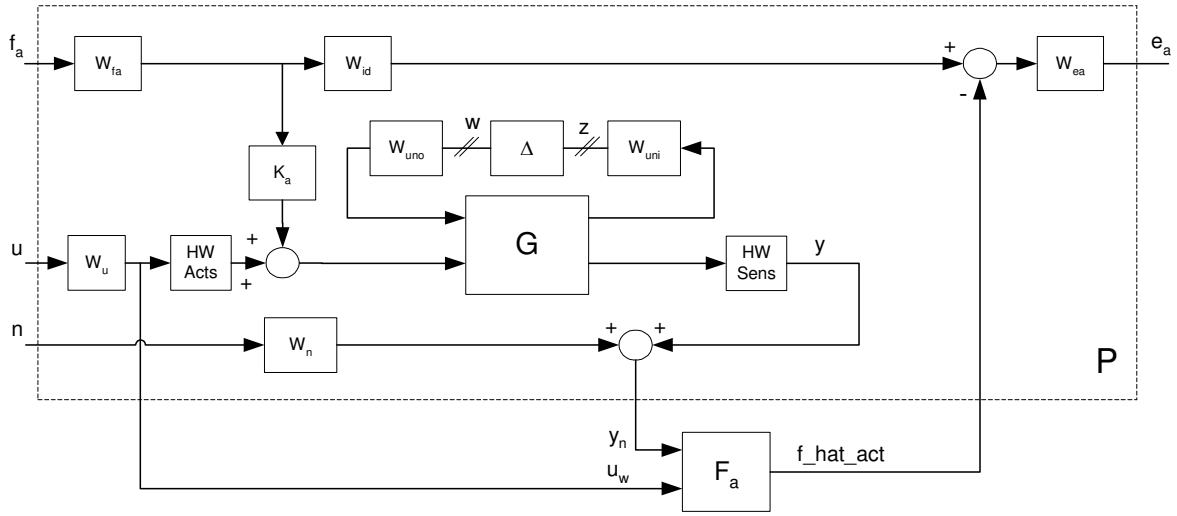

Figure 13. Longitudinal H-infinity FDI filter design interconnection.

2. Yaw rate sensor fault

The lateral FDI design problem is depicted in Figure 14. Here the plant model in LFT form is that for the lateral plant response at the chosen design point (trim point). Consistent with the lateral model of the vehicle, here the FDI filter takes as input the lateral actuator commands (effective outboard aileron, effective inboard aileron, rudder, RCS-x, engine 1 yaw gimbal, engine 2 yaw gimbal, engine 3 yaw gimbal) and a subset of the lateral model outputs, being roll rate p, yaw rate r, sideslip angle β and bank angle σ. Note that the LFT plant model includes all seven lateral states.

A solution to the FDI problem depicted in Figure 14 can be found using H-infinity design theory. The designed FDI filter F_s then takes 11 inputs (7 control inputs and 4 plant outputs) and outputs the scalar estimate of the fault acting on the yaw rate sensor.

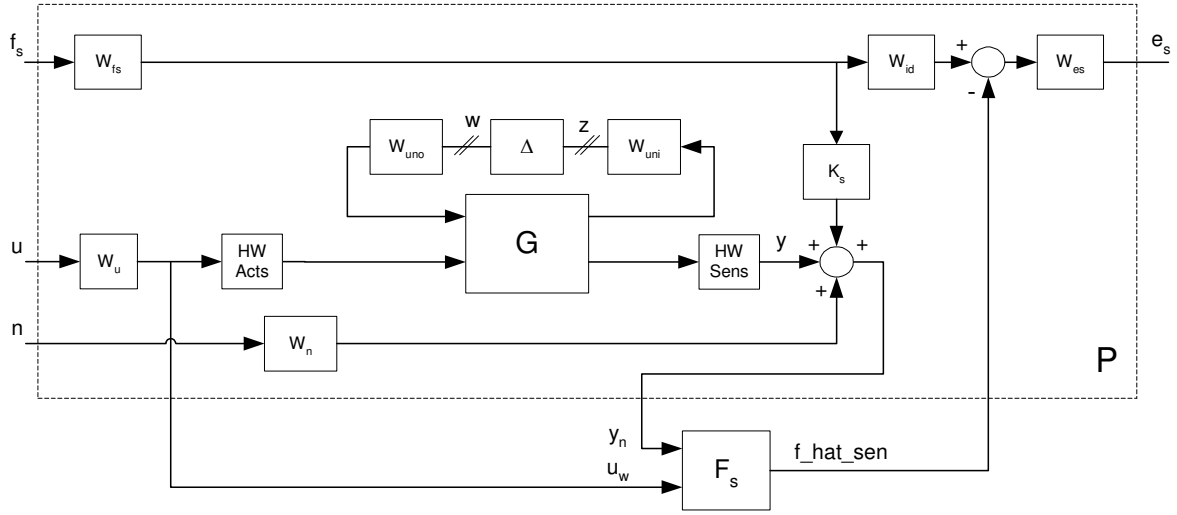

Figure 14. Lateral H-infinity FDI filter design interconnection.

3. Filter Construction

Filters are designed for the lateral and longitudinal FDI problems based on the H-infinity FDI design problems described in the previous section. LTI GNC-FDI filters were designed using standard H-infinity design tools, such as the Matlab *hinfsyn* algorithm.

The design points (trim points) over the 130 second ascent flight period at which the GNC-FDI filters were designed differ between the longitudinal and lateral design problems. For the longitudinal design problem, it was found that 22 design points at different values of the scheduling variable consumed mass were required to cover the ascent period. For the lateral design problem, 20 design points were chosen. These design points covered the full 130-second flight period, being denser over the first 60 seconds of flight.

4. LTI Filter Scheduling

The point-design LTI GNC-FDI filters were scheduled to extend their local FDI capabilities over the full ascent flight period considered. A simple linear scheduling of the filters was performed between the design points. While this scheduling approach is ad-hoc, it was found to work well in general, in part because the GNC-FDI filters were designed to be locally robust. For the scheduling variable, consumed fuel mass was chosen.

The scheduling of the lateral GNC-FDI filters over the full flight period was achieved in a straightforward manner due to the similarities in the filters quantitative and qualitative features. Subsequently the resulting gain scheduled filter represents an effective extension of good local properties of the point-design LTI filters over the full flight period. This is supported in the testing shown in Section IV.

The scheduling of the longitudinal FDI filters over the full flight period was found to be difficult in certain parts of the flight period. Specifically, over the first 50 seconds of the flight, where the qualitative properties of the vehicle dynamical response changes abruptly (ie complex stable to real unstable modes etc as discussed in Section III.D), it was difficult to extend the good local properties of the point-design LTI filters (This is also true to a lesser extent over the latter period from 100 to 130 seconds). Hence over this period of the flight, the capabilities of the scheduled longitudinal FDI filter may be slightly reduced compared to the local LTI filter designs used as the basis for the scheduling.

Remark: It is possible that the use of more rigorous scheduling approach would better allow for the extension of the good local properties of the point-design LTI filters over the full flight period. This is particularly the case for the longitudinal GNC-FDI filters.

5. Design of thresholding and isolation logic

The FDI signal (fault estimate) provided by the designed GNC-FDI filter should be an accurate indication of the fault occurrence, strength and dynamic, but due to uncertainty it cannot be perfectly decoupled from the effects of the exogenous signals on the system, with noise, control commands and disturbances all coupling to the FDI signal. Given this situation, to provide a fault diagnostic signal that does not provide significant false fault detections, it was chosen to process the fault estimate signal through an on-line fault thresholding algorithm. This is standard practice and the algorithm employed is this work similar to that described in Ref.10.

6. Filter implementation

The complete fault diagnosis algorithm is comprised of two parts: the FDI filter that provides a fault estimate based on the Hopper vehicle commanded inputs and measured outputs; and an on-line fault thresholding algorithm that further determines if a fault is active based on the relative absolute values of the fault estimates and an estimate of the coupling from control commands and noise to the fault estimate.

The designed FDI filters are of an order equal to the vehicle model and weighting filters. Prior to scheduling, these were reduced to 6th order for the longitudinal filters and 5th order for the lateral filters using Hankel model reduction techniques. The on-line fault thresholding algorithm requires additional processing, being of 2nd order and possessing several summation, absolute value and comparison operators.

IV. FDI Filter Testing and Robustness Analysis

The capabilities and robustness of the GNC-FDI filters were assessed in the time-domain via a Monte-Carlo (MC) campaign, performed by randomly varying the uncertainty present in the system. In the MC campaign, 1000 simulation runs were performed for each fault (sensor and actuator) using a functional engineering simulator for the Hopper RLV. Hence the filters. The features of the model in the simulator are described in Ref.1 and can be summarised as: full 6 DoF nonlinear RLV dynamics; high-fidelity EADS-ST Hopper aerodynamic database; 1962

USA atmospheric model; magnitude and rate limited actuators; completely automated simulation over the full re-entry trajectory; NDI controlled; errors and delays on consumed fuel mass estimate.

The results of the MC campaigns are shown in Figures 15, 16 and 17 for the sensor and actuator faults. Note that the results show both the actuator and sensor fault estimate for all runs in the campaign, irrespective of the fault, as both filters are always active. Note also the unit of these figures is radians.

Figure 15 shows that for the yaw rate sensor bias fault of 5 degrees/sec, acting from 50 to 100 seconds of the ascent flight, the fault estimate signal responds rapidly to the fault effect, with fault detection and isolation achieved quickly. The fault estimate is seen to also track the abrupt fault dynamic, with very accurate steady-state tracking. The transients seen in the fault estimate, both when the fault is activated and when it is deactivated, are due to the strong effect of this large and abrupt fault on the vehicle's behaviour under closed-loop control. Some false alarms are seen for the actuator fault estimate. None are seen for the sensor fault estimate.

Figure 16 shows that for the yaw rate sensor drift fault of 0.01 degrees/sec/sec, acting from 0 to 130 seconds of the ascent flight, the fault estimate signal responds relatively quickly to the fault effect, with fault detection and isolation achieved once the fault strength is greater than about 0.15 degrees/sec (the threshold level). The fault estimate is seen to also accurately track the fault dynamic, with accurate steady-state tracking. One false alarm is seen for the actuator fault estimate.

Figure 17 shows that for the engine 2 pitch gimbal bias fault of 5 degrees, acting from 50 to 100 seconds of the ascent flight, the fault estimate signal responds rapidly to the fault effect, with fault detection and isolation achieved quickly. The fault estimate does not track the fault dynamic in this case. Some false alarms are seen for the actuator fault estimate. None are seen for the sensor fault estimate. The fault estimate is also seen to respond strongly to the removal of the fault effect.

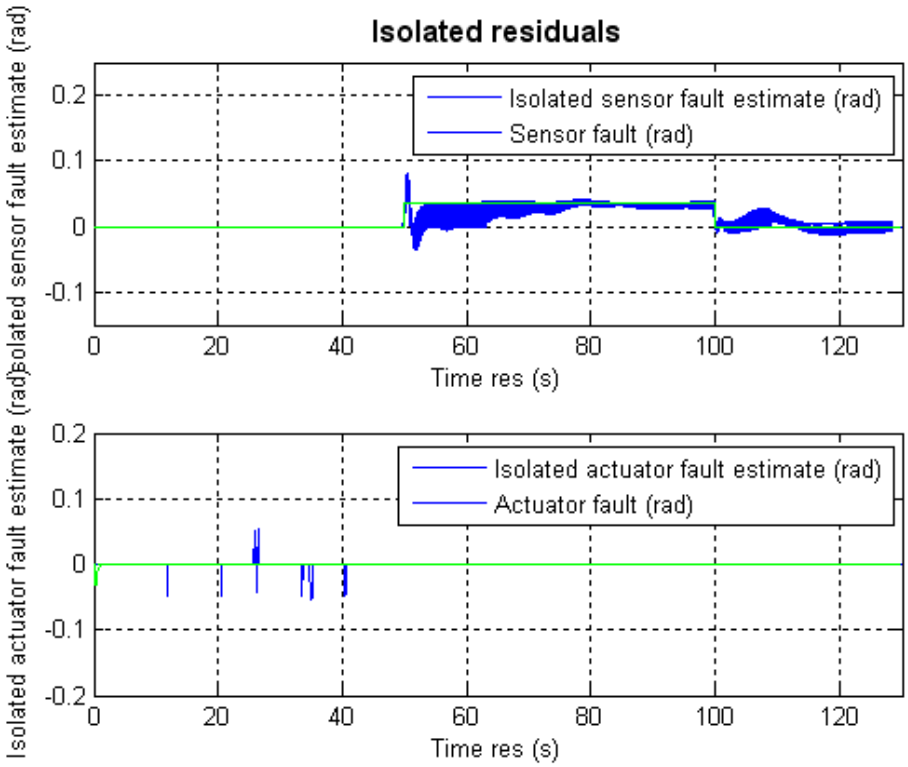

Figure 15. Isolated fault estimates for 1000 run MC campaign for the yaw rate sensor bias fault.

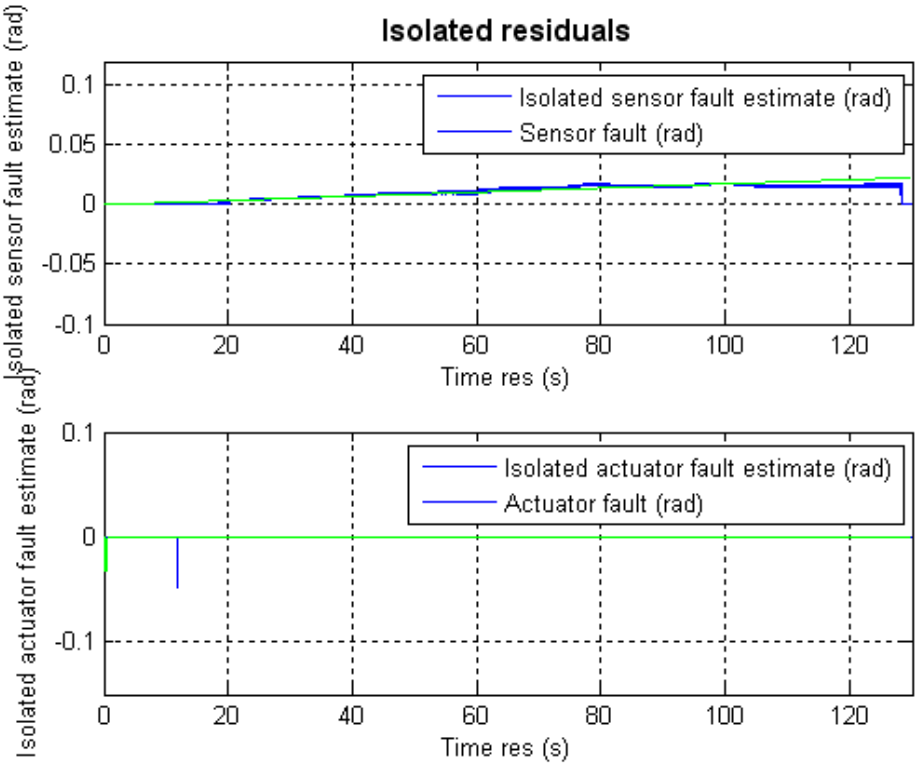

Figure 16. Isolated fault estimates for 1000 run MC campaign for the yaw rate sensor drift fault.

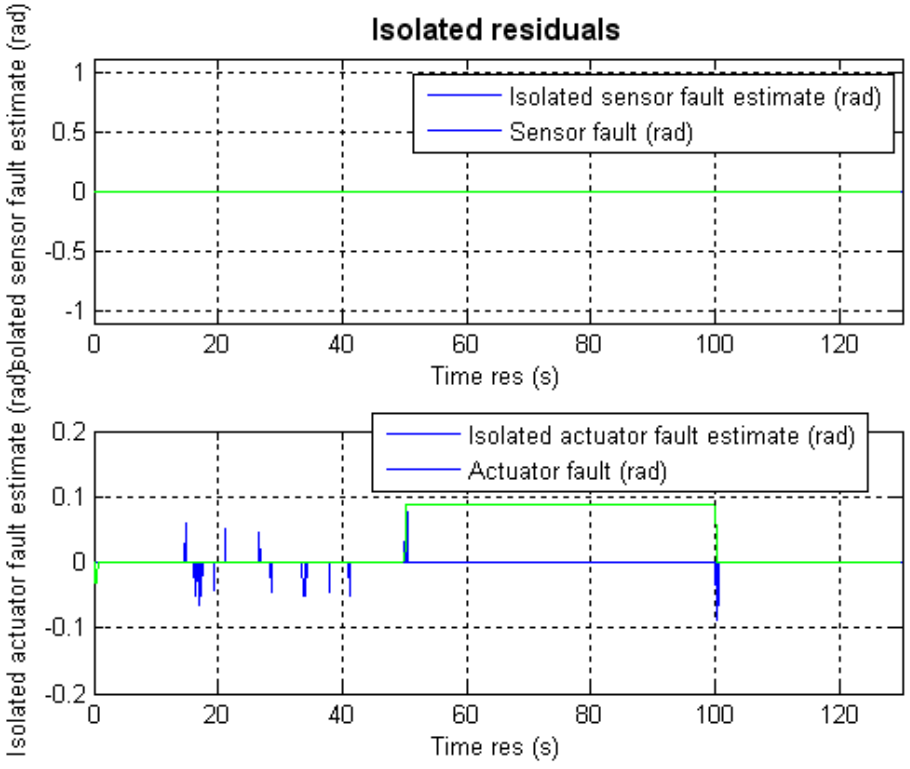

Figure 17. Isolated fault estimates for 1000 run MC campaign for the engine 2 pitch gimbal bias fault.

H. Performance Indices and Statistical Results Analysis

To assess the effectiveness of the designed GNC-FDI filters, performance indices (statistical measures) of the FDI results are employed. The selection of the performance indices for FDI performance assessment has been made by taking into account relevant aspects of failure detection performance for a GNC system in an ascent scenario. In the time domain, detection time is a very important indicator. Regarding the presence of model uncertainty, robust performance should also be addressed. In addition, as the effects of the introduced faults are not always known a priori, it is necessary to employ performance indices that can be applied to arbitrary dynamic signals. The energy ratios for fault estimation performance assessment detailed below are suitable for use with such signals.

7. Performance Indices for Fault Detection

The following performance indices are employed for fault detection:

Time-domain performance: The main parameters when assessing time-domain performance are:

Detection Time (t_{dt}): It is defined as the time from the occurrence of a fault to when the fault is effectively detected. This is a key index to identify time critical faults.

True Detection Rate (r_{td}): It is defined as the percentage of time that the fault is being correctly detected with respect to the time it appears within the system.

False Detection Rate (r_{fd}): It is defined as the percentage of time that the fault is being incorrectly detected with respect to the time a fault is being declared active.

Robust detection performance: Regarding indices related to robust detection performance. The following can be mentioned:

Detection ratio (r_d): It is defined as the percentage of correct detections n_c with respect to the total number of MC simulations n. That is,

$$r_d = \frac{n_c}{n} \times 100$$

False alarm ratio (r_{fa}): It is defined as the percentage of false alarms n_{fa} with respect to the total number of MC simulations n. That is,

$$r_{fa} = \frac{n_{fa}}{n} \times 100$$

8. Performance Indices for Fault Estimation

The following performances indices are used for fault estimation:

Normalised mean estimation error over the fault period (e_{nm}): The performance of the fault estimation is evaluated via the normalised mean of the estimation error over the fault period. This is the mean difference between the fault signal and estimate of the fault signal over the time period the fault is active, normalised by the magnitude of the fault, as shown below, where t_{f1} and t_{f2} are the start and end times for the fault, respectively, and f_m is the magnitude of the fault.

$$e_{nm} = \frac{1}{f_m} \times \frac{\int_{t_{f1}}^{t_{f2}} \left| f - \hat{f} \right|}{t_{f2} - t_{f1}}$$

True energy ratio (r_{et}): It is defined as the percentage of the energy in the fault estimate signal ($\hat{f}$) relative to the energy in the fault (f) over the time period that the fault is acting on the system.

$$r_{et} = \frac{\left| \hat{f} \right|_2}{\left| f \right|_2} \times 100$$

False energy ratio (r_{ef}): It is defined as the percentage of the energy of the fault estimate signal ($\hat{f}$) corresponding to a false fault detection ($\hat{f}_{false}$) over the time period that the FDI algorithm is declaring that a fault is acting on the system.

$$r_{ef} = \frac{\left|\hat{f}_{false}\right|_2}{\left|\hat{f}\right|_2} \times 100$$

Using these measures of performance, the results of the Monte-Carlo campaigns of 1000 runs for each fault case can be summarised as detailed in Table 1, Table 2 and Table 3.

Table 1. MC 1000 run Yaw Rate Sensor Bias Fault Performance Indices.

Yaw Rate Sensor Bias Fault (5 deg/s peak amplitude, 1000 MC simulations)								
Robust FD &FI Performance			Time Domain FD Performance			Time Domain Fault Estimation Performance		
Sensor		Actuator						
Detection ratio	False alarm ratio	False alarm ratio	Average Detection time	Average True detection rate	Average False detection rate	Average Normalised mean estimation error	Average True Energy Ratio	Average False Energy Ratio
100 %	0 %	1%	3.54e-3 s	97.92 %	0%	26.90 %	82.90 %	0%

Table 2. MC 1000 run Yaw Rate Sensor Drift Fault Performance Indices.

Yaw Rate Sensor Drift Fault (0.01 deg/s/s, 1000 MC simulations)								
Robust FD &FI Performance			Time Domain FD Performance			Time Domain Fault Estimation Performance		
Sensor		Actuator						
Detection ratio	False alarm ratio	False alarm ratio	Average Detection time	Average True detection rate	Average False detection rate	Average Normalised mean estimation error	Average True Energy Ratio	Average False Energy Ratio
100 %	0 %	0.1 %	14.11 s	87.47 %	0%	NA (*)	92.72 %	0 %

(*) Not applicable to a dynamic fault.

Table 3. MC 1000 run Engine 2 Pitch Gimbal Bias Fault Performance Indices.

Engine 2 Pitch Gimbal Bias Fault (5 deg peak amplitude, 1000 MC simulations)								
Robust FD &FI Performance			Time Domain FD Performance			Time Domain Fault Estimation Performance		
Actuator		Sensor						
Detection ratio	False alarm ratio	False alarm ratio	Average Detection time	Average True detection rate	Average False detection rate	Average Normalised mean estimation error	Average True Energy Ratio	Average False Energy Ratio
99.4 %	1.2 %	0 %	0.23 s	0.45 %	0.29 %	99.46 %	4.06 %	0.38 %

I. Results Summary

The results shown in Fig .15 and Fig.16, and summarised in Table 1 and Table 2, show that the yaw rate sensor GNC-FDI filter performs very well, with very good FDI capabilities seen for the bias and drift fault types for all 1000 simulation cases in the MC campaign. Fast detection and isolation is achieved in all cases. Accurate fault estimation is also achieved for both bias and drift faults. It is evident that the yaw rate sensor GNC-FDI filter provides highly robust FDI and fault estimation capabilities.

The results shown in Fig .17 and summarised in Table 3 show that the engine 2 pitch gimbal actuator GNC-FDI filter performs acceptably for the bias fault, with very good FDI capabilities seen for all 1000 simulation cases in the MC campaign. The filter provides fast detection and isolation for all test cases. However, accurate fault estimation is not achieved, as the filter does not provide for steady-state tracking of the fault dynamic. Additionally, the level of false alarms is not negligible and is clearly higher than 0 false alarms for the sensor fault estimate. It is evident that

the engine 2 pitch gimbal actuator GNC-FDI filter provides highly robust FDI capabilities for the bias fault. Very limited fault estimation capabilities are provided.

Remark: Other fault types were tested, with the results not shown here. This included actuator LIP and sensor dead faults. For the sensor dead fault, the performances were equivalent to that seen above, but due to the dynamical fault characteristics, the results are more difficult to show. As mentioned previously, due to the engine gimbal redundancy, the actuator LIP fault effects were easily accommodated and were too small to be detected.

V. Conclusion

In this paper the design and evaluation of GNC-FDI filters for fault detection and isolation (FDI) on the NDI controlled Hopper RLV vehicle during ascent was presented. The fault scenarios considered the focused time period of 130 seconds from the start of the ascent trajectory for the Hopper RLV. The work described the use of an H-infinity FDI filter design approach for the synthesis of open-loop GNC-FDI filters based on linearised models of the nonlinear ascent vehicle.

The performance of the GNC-FDI filters was evaluated using simulation campaigns on a high fidelity Hopper RLV simulator. The GNC-FDI algorithms were tested by introducing faults in the yaw rate sensor and engine 2 pitch gimbal actuator, for which they were designed. The evaluation considered a range of fault types; persistent faults (bias) and slowly developing faults (drift). Testing was performed using a MC campaign of 1000 shots drawn randomly within the uncertainty range of the system. The results of the evaluation were positive and, within the context of the HMS study, the design of effective GNC-FDI algorithms for the vehicle is considered to have been achieved.

For the Yaw rate sensor fault results:

- The GNC-FDI algorithm for the detection and isolation of faults in the yaw rate sensor showed excellent capabilities in all cases, with fast detection and isolation for the bias and drift fault types achieved robustly and with no false alarms.
- The capability of the GNC-FDI algorithm to estimate of the fault effects was very good in all cases.
- Overall the GNC-FDI algorithm for the detection and isolation of faults in the yaw rate sensor is considered to be highly applicable.

For the Engine 2 pitch gimbal actuator fault results:

- The GNC-FDI algorithm for the detection and isolation of faults in the engine 2 pitch gimbal actuator showed good capabilities in all cases for the bias fault, with fast detection and isolation achieved robustly with only minor false alarms.
- The capabilities of the GNC-FDI algorithm to estimate the fault effects of the engine 2 pitch gimbal actuator were not good, due to the specific dynamic properties of the vehicle in longitudinal motion; in particular, the high sensitivity of the trimmed vehicle's longitudinal stability to vehicle uncertainties and parameter variations.
- Overall the GNC-FDI algorithm for the detection and isolation of faults in the engine 2 pitch gimbal actuator is considered to be acceptable.

The designed GNC-FDI algorithms were considered to perform very well. It is however clear that further maturation of the FDI design method proposed is required to provide for improved fault detection and isolation capabilities for vehicles whose stability characteristics vary rapidly and/or are particularly sensitive to uncertainty and parameter variation. This is particularly the case if improved fault estimation capabilities are to be provided.

Acknowledgments

This worked was performed within the European Space Agency (ESA) study "Health Management for Reusable-space Transportation". The authors would especially like to thank Eric Bornschlegl of ESA ESTEC, the technical officer for the HMS study, and Alexander Schwientek, Wolfgang Belau and Josef Sommer of EADS Astrium Space Transportation, the leaders of this study and who also provided the model of the Hopper RLV.

References

[1] Marcos, A., Peñín, L.F., Caramagno, A., Sommer, J., Belau, W., "Atmospheric Re-Entry NDI Control Design for the Hopper RLV Concept," *Proceedings of the 17th IFAC Symposium on Automatic Control in Aerospace*, Toulouse, July 2007.

[2] Kerr, M.L., Marcos, A., Peñín, L.F., "Development of an FDI Filter for the Hopper RLV during Re-entry," *Proceedings of the 7th IFAC Symposium on Fault Detection, Supervision and Safety of Technical Processes*, Barcelona, July 2009.

[3] Kerr, M.L., Marcos, A., Peñín, L.F., and Bornschlegl, E., "Gain-Scheduled FDI for a Re-entry Vehicle," *Proceedings of the AIAA Guidance, Navigation and Control Conference and Exhibit*, Hawaii, 2008.

[4] Augustin, R.M., Mangoubi, R.S., Hain, R.M., Adams, N.J., "Robust failure detection for reentry vehicle attitude control systems," *Journal of Guidance, Control, and Dynamics*, Vol. 22, No. 6, 1999.

[5] Castro H., Bennani S., Marcos A. "Robust filter design for a Re-entry Vehicle," *Proceedings of the 7th International Conference on Dynamic and Control of Systems and Structures in Space*, UK, July, 2006.

[6] F. Cazaurang, V. Morio, A. Falcoz, D. Henry, A. Zolghadri, "New model-based strategies for guidance and health monitoring of experimental reentry vehicles", International Review of Aerospace Engineering. Vol. 1 (10). 2008.

[7] Marcos, A., De Zaiacomo, G., Peñín, L.F., Bornschlegl, E., "Fault Analysis for Robust FDI Design During RLV Ascent and Re-entry Phases," 7th International ESA Conference on Guidance, Navigation and Control Systems. Tralee, Ireland, June2008.

[8] Chen, J., Patton, R.J., *Robust Model-based Fault Diagnosis for Dynamic Systems*, Kluwer Academic Publishers: Dordrecht, 1999.

[9] Seron, M.M.; Goodwin, G.C., "Design limitations in linear filtering", Proceedings of the IEEE Conference on Decision and Control, 1995, pp. 1519 - 1524.

[10] Kerr, M.L., Marcos, A., Peñín, L.F., Brieger, O., Postlethwaite I., and Turner, M.C., "Piloted Assessment of a Fault Diagnosis Algorithm on the ATTAS Aircraft," *Proceedings of the AIAA Guidance, Navigation and Control Conference and Exhibit*, Chicago, 2009.